SvedbergOpen
DISSEMINATION OF KNOWLEDGE

International Journal of Artificial Intelligence and Machine Learning

Publisher's Home Page: https://www.svedbergopen.com/

Research Paper Open Access

Cloud assisted Multimodal Lung Cancer Classification Using an explainable Deep Learning approach

Gottumukkala Thanmaya Tejaswi[1], Nulaka Srinivasu[2], Pardha Saradhi Varma Gottumukkala[3]

[1]Research scholar, Department of Computer Science and Engineering, Koneru Lakshmaiah Education Foundation, Vijayawada, Andhra Pradesh-522302. India, ORCID: 0009-0004-6811-6867, Email: thanmayatejaswi@gmail.com

[2] Professor, Department of Computer Science and Engineering, Koneru Lakshmaiah Education Foundation, Vijayawada, Andhra Pradesh -522302. India, Email: srinivasu28@kluniversity.in, ORCID: 0000-0002-9593-3916

[3] Professor, Department of Computer Science and Engineering, Koneru Lakshmaiah Education Foundation,Vijayawada, Andhra Pradesh -522302. India, Email: gpsvarma@gmail.com, ORCID: 0000-0002-4885-1678

Abstract

Lung cancer ranks as the most common cause of death among all cancer types globally. Conventionally, CT scans and MRI were utilized to detect the lung modules, but it is time consuming and prone to errors, so this proposed model developed a novel deep learning approach to classify the lung cancer, which utilizes a PET, genomic, and clinical images to classify the lung modules. Initially, missing values are balanced utilizing mean imputation, then the data is normalized using min-max scaling. In the pre-processed images, the features are extracted employing PyRadiomics, Principal Component Analysis (PCA), and t-distributed stochastic Neighbor Embedding (t-SNE), which is utilized to reduce the noise. Additionally, the deep features are extracted employing Residual AlexNet, and the clinical data is encoded using One-hot encoding. Additionally, the Explainable cross-module attention deep fusion network pruning transformer (CDF-NPT) framework is used to classify the output. Shapely Additive Explanation (SHAP) is the framework utilized for feature attribution. Finally, the data is encrypted using a Secured dual stage encryption system technique using ElGamal ECC to secure the patients records. Further, the encrypted data is stored in the cloud platform successfully. Performance of this proposed system is evaluated utilizing metrics such as accuracy, precision, recall, F1-score, Encryption time, Execution time, ROC curve, Training and testing accuracy, and so on. The accuracy of this proposed model is 98.47% for TCGA and 99.01 % for the TCIA dataset, and the encryption time of 69 ms and 64 ms, respectively. The overall results indicate the proposed model outperforms the existing models.

Keywords: Deep fusion network pruning, Residual AlexNet, SHAP, ElGmal ECC, distributed stochastic, PyRadiomics.

1. Introduction

Lung cancer (LC) poses a significant worldwide medical concern, as it is the primary cause of deaths caused by cancer. Identifying cancer cells at an early stage is essential to avoid serious outcomes [1]. When body parts begin to produce unhealthy cells, these cells can travel across the body and ultimately lead to fatal outcomes [2]. Detection of cancer involves a blood analysis, radiographic imaging, tissue sampling, and computed tomography scan, along with physical assessment of the individual [3]. Historically, the identification of cancer depends on its characteristics, such as surface pattern, hue, and form of the abnormal growth. The attributes depend on the specific case, because just looking at color, texture, or shape is not enough to accurately determine what type of disease is present [4].

Lung cancer is conventionally divided into small cell type (SCLC) and non-small cell type (NSCLC) [5]. Due to the technology improvements, several deep learning (DL) techniques are employed to identify LC, including Copy Number Variation (CNV), acquired genetic alterations, and DNA modification studies of the tumor's genetic material [6]. Various scanning techniques like radiographs, magnetic field imaging (MRI), positron Scan

(PET), as well as Computed Tomography (CT) have been used to identify lung lumps. These diagnostic tools assist in the early detection of abnormal growths in the lungs [7]. Due to the recent advancements in deep learning based image processing, two specialized 3D hybrid connection networks (CMixNet models) were used to categorize nodules [8]. Genetic activity analysis has offered important insights into gene functions and illustrates the present biological condition of the cellular structure.

It has been employed to assist in the early identification as well as forecast of outcomes for several types of cancer [9]. The SVM model was applied to differentiate lung cancer categories, but SVM can struggle with large datasets and nonlinear relationships unless carefully tuned and kernel functions are well-chosen [10]. CNNs are used to detect patterns, whereas Vision Transformers (ViTs) analyze distant connections among image segments. CNN may miss global context, and ViTs require large datasets [11]. Typically, a Computer Assisted lung tumor identification system involves image enhancement, isolating the target area, and choosing relevant attributes, but such systems may suffer from reduced accuracy due to noise across different datasets [12]. Several conventional ML methods are found in prior research to help with lung tumor identification and categorization, such as SVM, which can limit the system's adaptability and accuracy [13].

The BICLCD-TSADL method analyzes medical scans to detect and categorize tumors in the large intestine and lungs, but it may struggle with accuracy when handling low-quality images [14]. Identifying lung cancer through a combined artificial intelligence approach by merging SVM and CNN, but this model may have a high computational cost and complexity due to integrating two distinct algorithms [15]. LC can be recognized using a variety of techniques, although identifying the affected area can be difficult due to low tumor region clarity and image capture mistakes [16]. The lung traits are analyzed using a combined CNN and long short-term memory model, which detects both healthy and irregular patterns in medical data, but this model may have limited interpretability for complex clinical data [17]. To overcome the prior limitations, this proposed system utilized a novel deep learning approach.

1.1 Motivation

Lung cancer is a situation where irregular cells replicate and expand into a mass tumor. These malignant cells may be transported from the lungs through the bloodstream or lymphatic fluid that encircles the lung tissue. Certain computer aided diagnostic systems utilized automatically extracted characteristics, while others employed manually designed attributes for spotting and categorizing the biological tissue. Manual features may lack adaptability, and learned features can require large datasets and training time. A Gabor filter is applied to increase the quality of the image. A Hopfield-based neural network and a fuzzy clustering technique are used for dividing sputum color visuals to identify lung tumors in their initial phases. This method can be sensitive to noise and may misclassify regions due to overlapping color intensities. Conventionally UNet model is employed to detect the lung tumors; it may give false results, so the segmented CT scans are given to the 3D CNN to classify the scans. As compared to the UNet model, a CT scan is more efficient in detecting lung nodules.

1.2 Objectives

- To integrate and preprocess multimodal data from TCIA datasets using normalization, outlier removal, and missing value handling techniques.
- To extract and refine high-quality features using radiomics, dimensionality reduction methods (PCA, t-SNE), and deep feature extraction via Residual AlexNet for robust cancer classification.
- To develop an explainable classification framework using the Cross-Module Attention deep fusion network pruning Transformer (CDF-NPT), along with SHAP for both global and instance-level model interpretability.
- To implement a dual-stage mechanism using Elgamal ECC encryption to securely store and share the classified patient records on a cloud platform.

This paper is organized from section 1 which presents the background and motivation of the study, section 2 explores and analyzes previous research related to this domain, section 3 elaborates on the detailed design and

implementation of the proposed approach, section 4 discusses the findings and evaluates the effectiveness of the method and section 5 concludes the study with key insights and suggestion for future advancements.

2. Related Work

This section explores the previous research work based on the Lung cancer classification system, which includes the methods, limitations, and performances.

Wankhade et al. [18] developed a deep learning (DL) model for cancer cell detection based on a hybrid neural network. DL networks are employed to extract data from CT scans. 3D-CNN is employed to increase the accuracy of lung nodule detection. This system utilized a LUNA 16 database to classify the data. This system attained an accuracy of 95% respectively. However, this suggested system needs to enhance the classification model by utilizing big data analysis.

Bhuiyan et al. [19] introduced a machine learning (ML) model to detect lung cancer; multiple models were trained to predict the disease, such as XGBoost, LightGBM, AdaBoost, Logistic Regression (LR), and Support Vector Machine (SVM). Among those models, XGBoost achieves a high accuracy of 96.92%. Although XGBoost provides high accuracy, it can be computationally intensive, especially with large datasets.

Srivastava et al. [20] suggested a Deep learning model of RCNN, which is utilized as a good model to detect critical data in medical imagery. Various techniques were utilized to detect the early stage of disease. The HFRCNN model, which starts by generating a collection that is classed and trained using CNN, is used to employ the second stage entity detector. This system achieved an accuracy of 97% respectively. However, this system needs to train the model on a large dataset.

Mamun et al. [21] suggested a Deep learning model of CNN, Inception V3, and ResNet were utilized, which utilized a CT based image for detecting lung cancer. These several models are compared with each other to evaluate the performance. The CNN model attained an accuracy of 92% respectively. However, this system needs to utilize advanced DL and ML models for better accuracy.

Naseer et al. [22] suggested a Machine learning model of SVM. This system utilized CT images for lung cancer detection (LCD). Where several convolution layers were employed to extract the features, such as seven convolutional layers, three pooling layers, and fully connected layers (FCL), this system attained 97.64% accuracy. However, this system needs to be realized on publicly available datasets.

Noaman et al. [23] suggested ML algorithms such as SVM, KNN, CatBoost, XGBoost, and decision trees to detect lung cancer. This system achieved an accuracy of 97.683% respectively. Further, this system utilized an LC2500 dataset to assess the classification performance of the models. However, this system needs to integrate different augmentation methods to reduce the processing time.

Verma et al. [24] suggested an Artificial Intelligence algorithms were used to detect lung cancer, simultaneously AI enhanced Low Dose computed tomography (LDCT) screening helps in early recognition of nodules. This system attained an accuracy of 95% in the early detection of lung modules. However, this system needs to implement advanced AI tools for better accuracy.

Ochoa-Ornelas et al. [25] suggested a deep learning model of CNN, MobileNetV2, and Lung adenocarcinoma (LAC) to detect the lung nodules. To enhance the model's classification LC2500 dataset was used. In the performance evaluation, this system achieved an accuracy of 98.11% respectively. However, this system needs to enhance the scope of the model's application.

Al-Jamimi et al. [26] suggested a machine learning algorithm of Recursive feature elimination with a SVM for feature extraction, the features are extracted using the XGBoost algorithm. This system achieved an accuracy of 98% respectively. However, this system needs to reduce the processing time. Table 1 illustrates the previous research analysis of the lung cancer detection system.

Table 1: Prior research analysis on early detection of Lung cancer

Author name and Reference	Methods	Performance	Disadvantages

Wankhade et al. [18]	Deep Learning, 3D-CNN	This system achieved an accuracy of 95% respectively.	This system needs to enhance the classification model by utilizing big data analysis.
Bhuiyan et al. [19]	XGBoost, LightGBM, AdaBoost.	XGBoost provides high accuracy.	It can be computationally intensive, especially with large datasets.
Srivastava et al. [20]	RCNN, HFRCNN	This system achieved an accuracy of 97% respectively.	This system needs to train the model on a large dataset.
Mamun et al. [21]	CNN, Inception V3, and ResNet	The CNN model attained an accuracy of 92% respectively.	This system needs to utilize advanced DL and ML models for better accuracy.
Naseer et al. [22]	SVM	This system achieved 97.64% accuracy, respectively.	This system needs to be implemented on publicly available datasets.
Noaman et al. [23]	KNN, CatBoost	This system achieved an accuracy of 97.683% respectively.	This system needs to integrate different augmentation methods to reduce the processing time.
Verma et al. [24]	Artificial Intelligence, LDCT	This system achieved an accuracy of 95% in the early recognition of lung modules.	This system needs to implement advanced AI tools for better accuracy.
Ochoa-Ornelas et al. [25]	CNN, MobioleNetV2	This system achieved an accuracy of 98.11% respectively.	This system needs to enhance the scope of the model's application.
Al-Jamimi et al. [26]	Recursive feature elimination with an SVM	This system attained an accuracy of 98% respectively	This system needs to enhance the model for multiple disease detection.

2.1 Problem Statement

Despite the advancements of various medical technologies, there are significant challenges and limitations in the medical fields; some system needs to enhance the classification model by utilizing big data analysis. [18], it can be computationally intensive, especially with large datasets. XGBoost, LightGBM, and AdaBoost were developed by [19] and lack in training using a large dataset. The RCNN model was suggested by [20]. There is no advanced model of DL that was used. The SVM model was introduced to identify lung cancer [22], where no proper augmentation and processing are high. A CatBoost model was developed by [23]; there are no advanced AI tools used, and it has low accuracy. LDCT was introduced to predict lung cancers by [24, 25], which needs to enhance the scope of the model's application. There are no DL techniques, and advanced ML techniques are used by [26].

3. Proposed Methodology

This paper proposes a Cloud assisted multimodal lung cancer classification using a deep fusion network pruning transformer. In contrast to single data, multimodal data gives high-performance results. Initially, genomic and clinical data are collected as input from the TCIA and TCGA datasets. Mean imputation is utilized to fill the missing values, and to remove the outliers statistical method is fused. Normalization is performed by using the min-max scaling. The features are extracted from the preprocessed images by utilizing PyRadiomics, principal component analysis (PCA), and t-Distributed Stochastic Neighbor embedding (t-SNE) is employed for noise reduction. The workflow of the Lung cancer classification model is depicted in Figure 1.

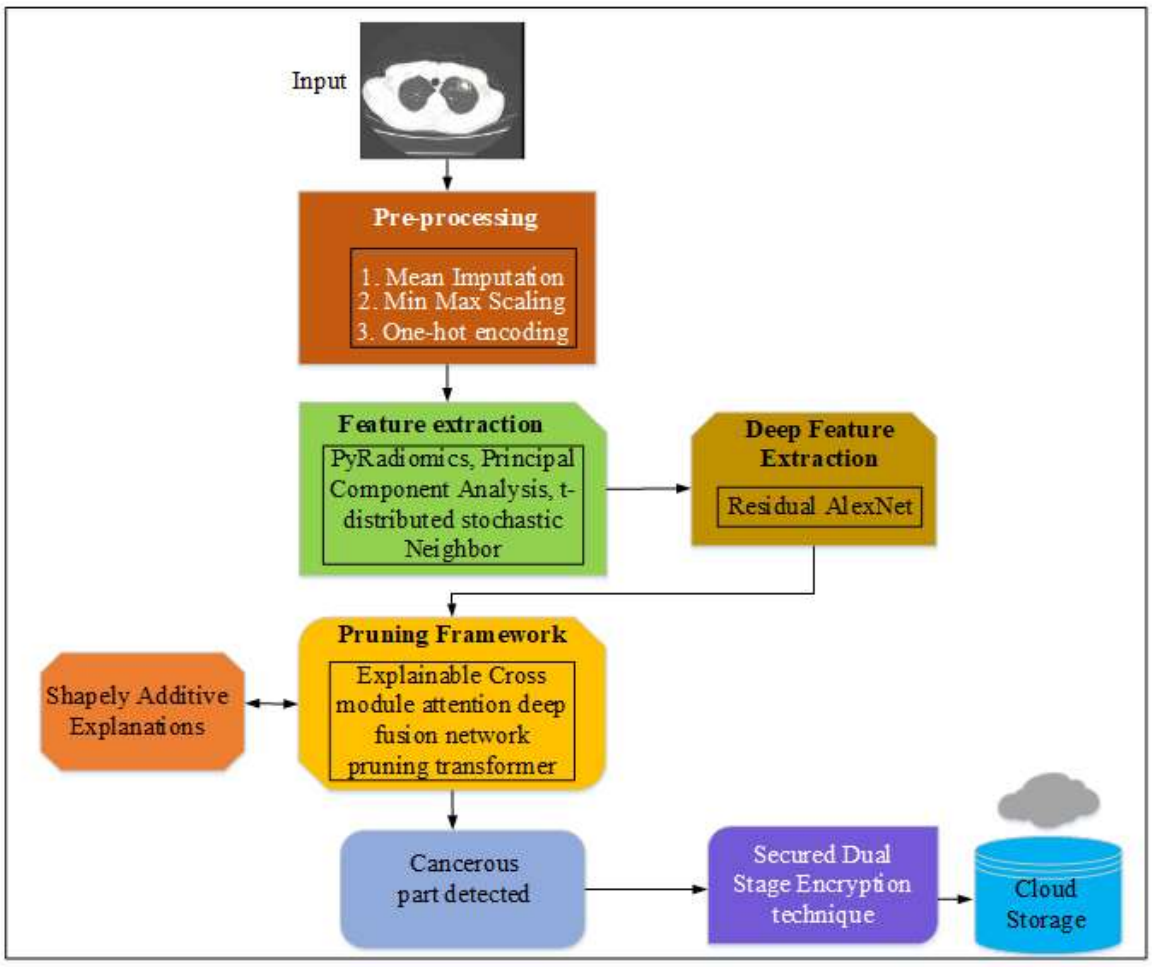

Fig. 1: Workflow of the Lung cancer classification model

Residual AlexNet is employed for deep feature extraction. Categorical data is encoded using one-hot encoding. Encoded data is categorized using an Explainable cross module deep fusion network pruning transformer. Shapley is a framework that works for both global and local explanations. The data is encrypted using Elgamal ECC to secure the patient records. Finally, the encrypted data is stored in the cloud.

3.1 Preprocessing

The raw genomic and clinical data are pre-processed by handling missing values and normalizing the data through mean value imputation (MVI) and min-max normalization. This step helps to improve the quality and maintain uniformity across multiple datasets.

3.1.1 Mean value Imputation

MVI is the most popular statistical based imputation to handle the missing values. The MVI demonstrates that when a value is missing in a dataset, this model fills the gap by taking the average of the other available values in the same feature.

$$\hat{v} = \frac{1}{m}\sum_{k=1}^{m} v_k \qquad (1)$$

here, $\hat{v}$ is the filled-in value, v_k is the existing known values, m is the amount of known values, and $\sum_{k=1}^{m} v_k$ signifies the total sum of all known values.

3.1.2 Min-Max scaling

In this model, all the data values, like gene expression level or clinical data and image intensities, are converted into a standard scale from 0 to 1. This process ensures consistency across different types of data and helps the model learn better by treating every feature fairly, especially when values vary widely in scale.

$$v' = \left[\left(\frac{v - v_{old\,\min}}{v_{old\,\max} - v_{old\,\min}} \right) * \left(v_{new\max} - v_{new\min} \right) + v_{new\min} \right] \quad (2)$$

here v' is the normalized value, v is the original value, $v_{old\,\min}$, $v_{old\,\max}$, is the minimum and maximum value among the dataset, $v_{new\max}$ and $v_{new\min}$ is the final normalized data ranging from [0,1].

3.1.3 One-hot encoding

One-hot encoding is a technique employed to convert definite (text-based) data, such as cancer type, tumor stage, or smoking status, into a format. Each label is turned into a binary vector. This vector has all zeros, except for a single '1' in the position that corresponds to the specific category. In each of these new features, the entries are marked with:

- 1 to show the presence of a category
- 0 to indicate its absence, Table 2 demonstrates the process of one-hot encoding.

Table 2: Process of One hot-encoding table

Tumor stage	Stage 1	Stage 2	Stage 3
Stage 1	1	0	0
Stage 2	0	1	0
Stage 3	0	0	1

3.2 Feature Extraction

In this section, features, texture, and shape or intensity are extracted from the normalized data by utilizing PyRadiomics and PCA, as well as the noise is reduced by utilizing t-SNE.

3.2.1 PyRadiomics

PyRadiomics is built in a modular manner to facilitate user interaction. The core component is the feature extractor module, which manages feature extraction and synchronizes the operation of various system components. Each type of feature is placed in its own module, and all of them are derived from a shared base class, which ensures a consistent structure and interface for feature extraction.

Additionally, the platform includes two supporting modules: generalinfo, which gives extra details about the extraction and includes them in the results. Image operations, which contain the image processing and filtering functions used before, are extracted. In addition to being used interactively in Python programs via the feature extractor module, PyRadiomics also allows users to run it directly from the command line. It offers two command line tools: PyRadiomics for processing a single image and PyRadiomicsbatch for handling multiple images at once. Both tools can take an optional configuration file to customize the feature extraction process. The output results can be easily given to various statistical analysis tools like R or SPSS. Additionally, PyRadiomics comprises a user-friendly graphical interface through the radiomics extension in 3D Slicer, making it accessible for users who prefer visual tools over coding.

3.2.2 Principal Component Analysis (PCA)

PCA is a method used to reduce the number of features in the dataset while keeping the most important information. In this proposed methodology, it is used to simplify high-dimensional data like gene expressions or radiomics features from the images. D is the dataset matrix that contains S samples and F features, for example, each sample could be a patient's data with 1000 gene expressions. PCA looks for a new direction called a projection vector c that can be used to remap data in a way that the new version p captures as much variation in the data as possible. $p = Dc$ is a linear transformation that is a compressed version of the original data.

$$\max_{C0} \frac{1}{S-1} p^T p = \max_{C} \frac{1}{S-1} c^T D^T Dc \qquad (3)$$

here, the principal component vector $p \in \mathbb{R}^F$ is also referred to as the score vector, which represents the transformed data in the new direction. Solving optimization problem (3) results in performing an eigenvalue decomposition, which helps to identify the principal constituents that seizure the most alteration in the lung cancer data is formulated as,

$$\lambda c = \frac{1}{S-1} D^T Dc \qquad (4)$$

3.2.3 t-Distributed Stochastic Neighbor Embedding (t-SNE)

In this proposed methodology t-SNE model is used to suppress the noise of the data. Given a dataset $D = \{d1, d2, ..dS\} \subset \mathbb{R}^v$ in a high dimensional space v, t-SNE is a technique that maps this data into a lower dimensional space $G = \{g_1, g_2, g_3, ..gs\}$ with dimension v' where $v' < v$. The goal of t-SNE is to ensure that if two data points d_1 and d_2 are near each other in the original dimension space, then their corresponding low-dimensional points g_1 and g_2 will also be located close together in the new space. The similarity among points d_j and d_k in the original space is represented by a probability value denoted as c_{jk}. Which is formulated as,

$$c_{j|k} = \frac{\exp\left(-\left\|d_j - d_k\right\|^2 / 2\sigma_j^2\right)}{\sum_{k \neq j} \exp\left(-\left\|d_j - d_k\right\|^2 / 2\sigma_j^2\right)} \qquad (5)$$

$$c_{jk} = \frac{c_{j|k} + c_{j|k}}{2S} \qquad (6)$$

$$r_{jk} = \frac{\left(1 + \left\|g_j - g_k\right\|^2\right)^{-1}}{\sum_{ku \neq l} \left(1 + \left\|g_{ku} - g_l\right\|^2\right)^{-1}} \qquad (7)$$

The value σ_j represents the bandwidth of the Gaussian distribution used to measure how likely the point c_k is to be a neighbor of the point c_j. This spread is selected in a way that ensures the perplexity (a measure of how many effective neighbors a point has) of the probability distribution c_j matches a specified value.

here, c_j refers to the conditional probability distribution that describes how likely all other points are to be neighbors of d_j.

T-SNE tries to position the points $\{g_1, g_2, .., g_S\}$ in a lower dimensional space in such a way that the difference between how the data points relate to each other in the original high-dimensional space (c) as well as in the reduced low dimensional space (R) is as small as possible. This difference is measured using a method called Kullback-Leibler (KL) divergence, which shows how much one probability distribution is not like another. Therefore, the impartial of t-SNE is to ensure that the neighborhood structure reflected in the new low-dimensional representation is identical to that of the original data.

$$P(G) = KL(C \| R) = \sum_{j \neq k} c_{j,k} \log \frac{c_{j,k}}{R_{j,k}} \quad (8)$$

Starting with a random initial guess for the low-dimensional points G, the t-SNE algorithm gradually improves the layout by reducing a specific cost function $P(G)$, which measures how different the current arrangement is from the desired one. This is done using gradient descent, a method that adjusts the points step-by-step in the direction that reduces, based on the gradient (i.e., slope or direction of fastest change).

$$\frac{\partial P}{\partial g_j} = 4 \sum \left(c_{j,k} - R_{j,k}\right) R_{j,k} W\left(g_j, g_k\right) \quad (9)$$

here, W is a global normalization constant,

$$W = \sum_{ku \neq l} \left(1 + \|gku - gl\|^2\right)^{-1} \quad (10)$$

Split the gradient into two parts

$$\frac{1}{4} \frac{\partial P}{\partial g_j} = \sum_{j \neq k} c_{jk} R_{jk} W\left(g_j - g_k\right) - \sum_{k \neq j} w_{jk}^2 W\left(g_i - g_j\right) \quad (11)$$

The first summation term, denoted as $X_{attr,j,}$ represents the pulling force that brings similar points together in dimensional space. The second summation term $X_{rep,j}$ represents the pushing force that keeps dissimilar points apart to prevent crowding. These two opposing forces help t-SNE arrange the data meaningfully by balancing closeness and separation.

3.2.4 Residual AlexNet

The AlexNet Convolution Neural Network (CNN) model includes techniques like batch normalization and max pooling to improve training and performance. The main distinction between a standard sequential CNN and a ResNet (Residual Network) includes shortest paths, also known as skip connections-which allow the input to bypass some layers and connect directly to later ones. This design enables those later layers to focus on learning only the difference (residual) from the input, rather than relearning everything. In fully connected layers, some information is lost as it passes through each layer, which can lead to a decline in data quality and negatively affect how well the model recognizes patterns. As a result, image detail may degrade, reducing the accuracy and efficacy of the classification. Figure 2 depicts the workflow of the AlexNet network.

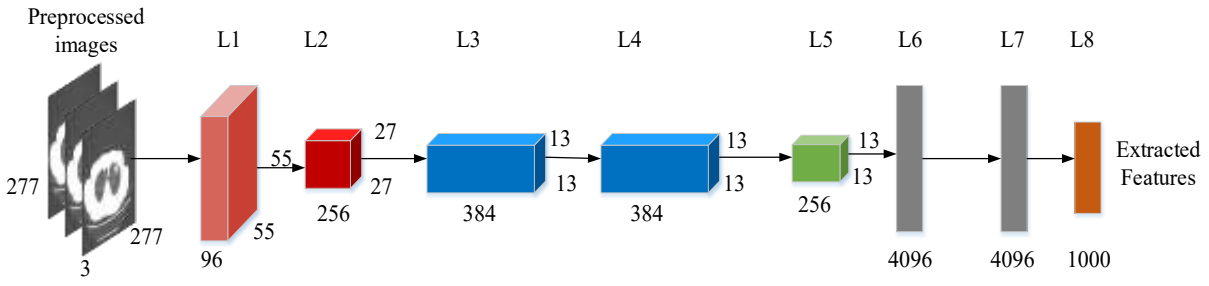

Fig. 2. Workflow of AlexNet Network

The pre-processed input data format is 227×227×2 pixels, where 227 pixels specify the height and width of each image, and the value 3 designates that the two types of data. The first two layers perform convolution, RELU activation, max-pooling, and normalization. The second layer process 256 feature maps using a 5×5 kernel and a stride of 1, similar to the first. The third and fourth layers apply only convolution and ReLU, while the fifth is like the first but without normalization. Its output is flattened into a vector as well as passed to a three-layer fully connected neural network. The first two dense layers have 4096 neurons, and the final layer with 1,000 features uses softmax to generate classification results.

ResNet helps to overcome the issue of information loss by allowing the original input data to flow directly to the output through shortcut connections. This method ensures that key characteristics are retained while maintaining the image's complete details. Training is made easier, faster, and the model learns more effectively because of the design, which just requires the network to acquire the alteration among input and output. In the original AlexNet model, ReLU is used as the activation function. This function helps avoid the vanishing gradient problem during back propagation and speeds up the training of the CNN and the standard ReLU function, respectively.

$$\mathrm{Re}\,Lu = \begin{Bmatrix} z, if & z > 0 \\ 0, if & z \le 0 \end{Bmatrix} \qquad (12)$$

here z is the input value to the activation function, which typically comes from the FCL. The model also applies both global max pooling and global average pooling methods to evaluate how various pooling strategies influence the model's recognition performance.

3.3 Classification

The extracted features are classified using an Explainable cross module attention based network fusion transformer. Initially, the extracted features are fed into the network pruning transformer module, and then the classified feature is given into cross module attention, and it is passed to the fully connected layer to the softmax, which gives the output as cancerous or non-cancerous.

3.3.1 Deep fusion Network pruning transformer

In this method, the output from the prior layer is fused with the network transformer. Fusion can be classified into input fusion, output fusion, and intermediate fusion. By utilizing concatenation and merging, fuse the information. In the output level, separate deep learning models can be applied to both datasets to extract features individually, which are then merged at a later stage.

Pruning is the process of removing unnecessary parts of a model, like unimportant features or tokens, to make the model lighter and faster without losing important information. In this research, pruning helps the deep learning network focus on only the most relevant lung cancer features, improving efficiency and reducing computation.

In this approach, a soft learnable mask $\widetilde{S}^{(i)}$ is used. This soft mask is created using the sigmoid function σ , which allows smooth adjustmentof which features are kept or reduced.

$$\tilde{S}^{(i)}(y_j) = \sigma\left(\frac{m^{(i)}(y_i) - \theta^{(i)}}{E}\right) \quad (13)$$

here, $\tilde{S}^{(i)}(y_j)$ is the score of the feature at layer j, $\theta^{(i)}$ is the learnable threshold for that layer, E is the temperature value that controls smoothness, σ and is the sigmoid function that softens the decision.

$$\tilde{y}_{out}^{(i)} = \tilde{S}^{(i)}(y^{(i)}) \cdot y_{out}^{(i)} \quad (14)$$

$$= \tilde{S}^{(i)}(y^{(i)}) \cdot LN\left(FFN(y_{MHA}^{(i)}) + y_{MHA}^{(i)}\right) \quad (15)$$

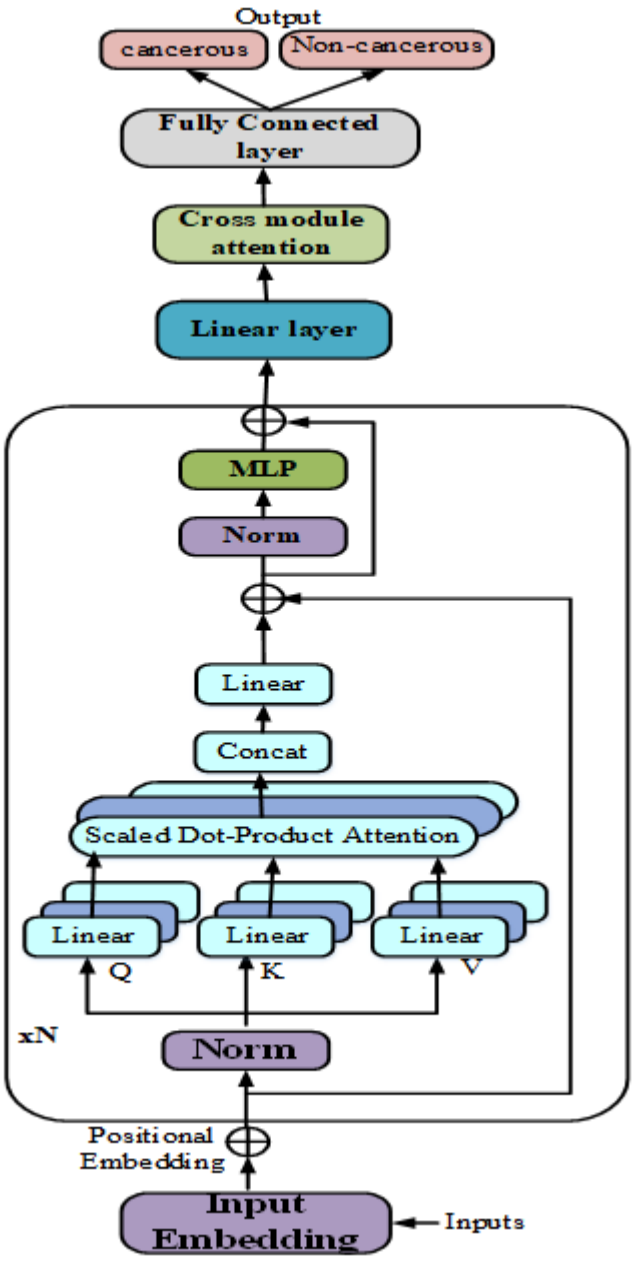

Fig.3: Workflow of Network Pruning Transformer

here, $y_{MHA}^{(i)}$ describes the output activation function of MHA in the layer i. The layer's output activation is nears zero while the significance score of the token y_i is below the threshold by a large margin. The threshold needs to be pruned again when the token gets a zero prominence score in the subsequent layer, i.e. $m^{(i+1)}\left(y_j\right)=0$

- Training model restrictions and a threshold on downstream asks with the soft pruning structure.
- Binarize the soft mask and fix the threshold.
- Follow-up fine-tuning of the model restrictions is performed,

3.3.2 Cross module attention

The core design of Cross Module Attention is structurally similar to the squeeze and excitation network, but with enhancements in its internal layout and the addition of a multi-feature selection mechanism. These improvements help in extracting more meaningful features and directing the model's focus specifically to the tumor region in the given lung scan. In this proposed methodology. Cross module attention is applied after each Feature Extraction Module within down sampling path of the network. Cross module attention relies on two main components. The first is the channel attention unit, which identifies and emphasizes the features that are most important for the task. The second is the feature selection module, which filters out less relevant or unnecessary information, allowing the network to focus on the most meaningful data. Output from the module is denoted as $H_j \in R^{v\times u}$. Then, Global Average Pooling GA_P as well as Global Max Pooling GM_P are applied to this output to compress the spatial information into summary values for further processing. The feature map from the module is denoted as α, the two outputs after pooling are,

$$\begin{bmatrix} \alpha GA_P = GA_P(\alpha) \\ \alpha GM_P = GM_P(\alpha) \end{bmatrix} \quad (16)$$

To simplify the above equation, the GA_P *and* GM_P compress each channel's spatial information to a scalar is expressed as,

$$\alpha GA_P, \alpha GM_P = \frac{1}{M}\left\{\sum_{S=1}^{M} z_j(D,S)\right\}_{D=1}^{D} \quad (17)$$

These are compressed descriptors that represent summary statistics of the feature map and help the network focus more accurately on the cancerous regions during classification.

here, $z_j(D,S)$ are individual components of the feature output $H_j \in R^{v\times u}$, where D represents the compressed summary of features from both pooling operations (average and max), capturing key information from the lung scan. Next, both pooled outputs (αGA_P and αGM_P) are passed through a shared neural layer, made of two fully connected (dense) layers and activation functions. This transformed the pooled values as follows:

$$\begin{bmatrix} x_{gap} = f_{sig}\left(M_2 f_{\mathrm{Re}LU}\left(M_1 \alpha GA_P\right)\right) \\ x_{gmp} = f_{sig}\left(M_2 f\,\mathrm{Re}LU\left(M_1 \alpha GM_P\right)\right) \end{bmatrix} \quad (18)$$

where, $f\,\mathrm{Re}LU$ applies a non-linear ReLU role is functional to capture complex patterns, f_{sig} applies a sigmoid role is useful to normalize the output between 0 and 1 as formulated in equation 16, M_1 and M_2 are learnable weight matrices used in the transformation.

$$f_{sig} = \frac{1}{1+e^{-z}} \quad (19)$$

Output of x_{gap} and x_{gmp} is f_{merg} formulated as,

$$f_{merg} = x_{gap} \cdot x_{gmp} \quad (20)$$

Figure 3 illustrates the workflow of crossover mutation.

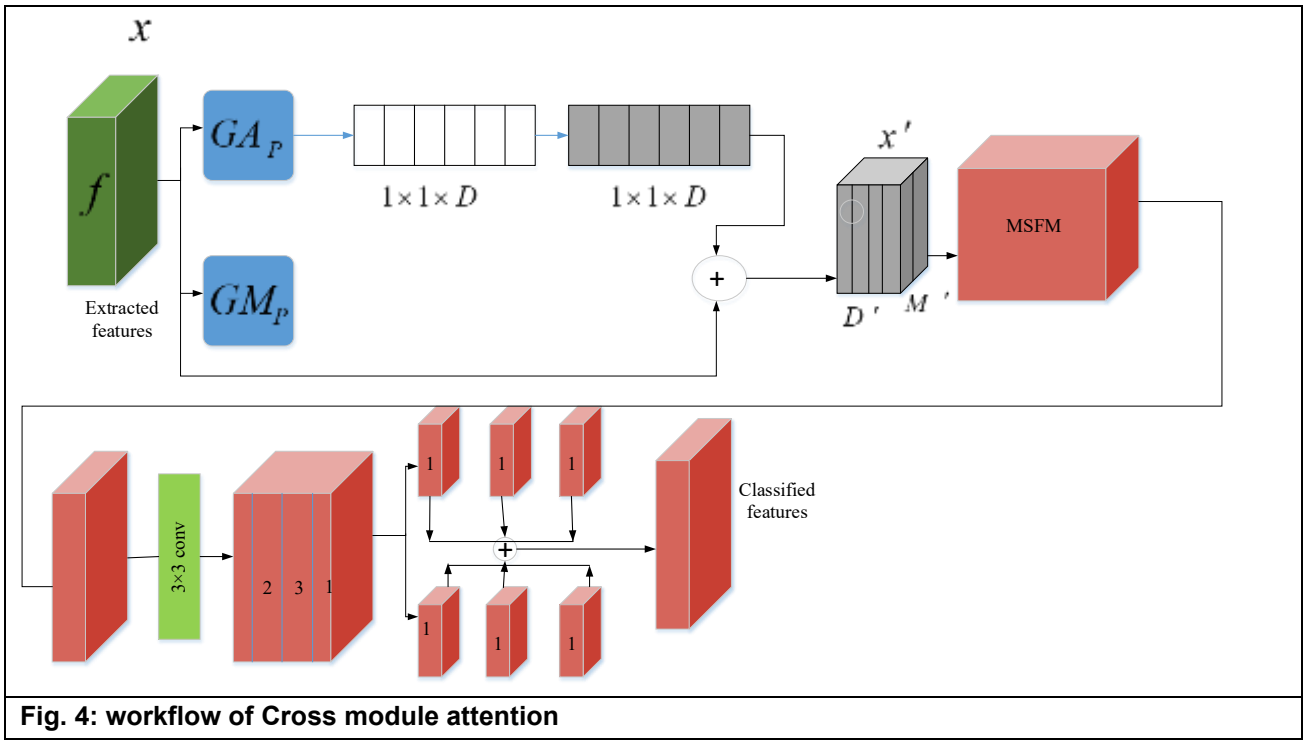

Fig. 4: workflow of Cross module attention

In the final step, the output from the channel module is created by applying a skip connection-based fusion that combines the refined features with the original input features z_j. This combination ensures that both the original image details and the enhanced attention-weighted features are preserved. Mathematically, this fusion is represented by,

$$f_{out} = \left\{ f_{merg}(D) \cdot z_i(D) \right\}_{D=1}^{D} \quad (21)$$

The output is sent to the Multi-scale Feature Selection module (MSFSM) to improve feature variety. MSFSM is designed symmetrically to seizure data at altered scales, enriching the feature set. The feature map x is split equally across channels into m parts, each having $\frac{1}{m}$ one of the original channels. These sub-maps are processed using 3×3 convolutional layers from either the left or right path. The result of each convolution is denoted as V_j^D, calculated as,

$$V_j^l \begin{cases} D_j^l(x) j = 1 \\ D_j^l\left(x_j + V_{j+1}^l\right) 1 < j \le n \end{cases} \quad (22)$$

$$V_j^s = \begin{cases} D_j^s\left(x_j\right) j = m \\ D_j^s\left(x_j + V_{j+1}^s\right) 1 \le j < m \end{cases} \quad (23)$$

Finally, the output V_j is calculated by merging V_j^l and V_j^s as follows,

$$V_j = V_j^l + V_j^s \quad (24)$$

The classified features from the transformer layer are fed into the cross module attention. By capturing the model relationship, the module increases the model's ability to differentiate cancerous or non-cancerous lung nodules.

3.4 Shapley Additive Explanation

The shapely value is a method used to fairly assign importance to each feature or input based on how much it contributes to the final prediction. It ensures that each data input, like clinical or gene expression, receives credit proportional to its impact on the model's decision. The shapely value is definite as follows:

$$\Phi(y_j) = \sum_{V \subseteq \{1,2,3,..R\} \setminus \{j\}} \frac{|M|!(R-|M|-1)!}{R!} \left[f_y(M \cup \{j\}) - f_y(M) \right] \quad (25)$$

where, R is the number of stakeholders. $\left[f_y(M \cup \{j\}) - f_y(M) \right]$ Describes the contribution of the entity j can be described as a marginal contribution, i.e. difference between the profit gathered by group M members only, $f_y(M)$ and that of both the entity j and the group members $f_y(M \cup \{j\})$. This calculation is repeated across all possible combinations of input features, and the shapely value is computed as the average impact each feature makes to the model's prediction, added to different combinations. Figure 4 illustrates the SHAP summary plot demonstrating the global impact of selected radiomics features on the proposed model's predictions. Figure 5 demonstrates the SHAP summary plot, demonstrating the global impact of selected radiomics features on this proposed model's predictions.

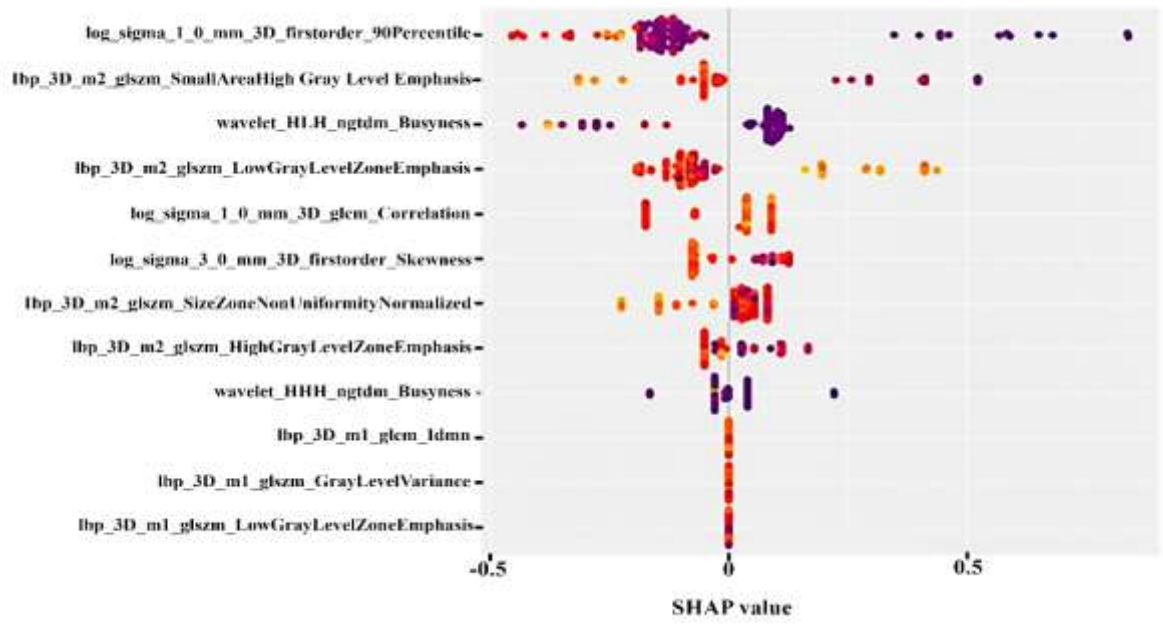

Fig. 5: SHAP summary plot demonstrating the global impact of selected radiomics features on this proposed model's predictions.

The SHAP summary plot illustrates the influence of individual radiomics features on the forecasts made by the proposed Multimodal lung cancer classification system. Top-ranking features such as log_sigma_1_0_mm_firstorder_90Percentile and small Area High Gray Level Emphasis show a strong influence on model decisions. Positive SHAP values shift the prediction toward the cancerous class while negative values support the non-cancerous class. Dot colors indicate actual feature values, red for high and purple for low. This

highlights how feature intensity affects classification outcomes. The analysis confirms that the model leverages key radiomics markers effectively for accurate detection. Overall, SHAP provides critical explainability and supporting clinical trust.

The Shapley method is unique because it's the only approach for assigning contribution scores that satisfies four key principles: Efficiency, symmetry, Linearity, and Null Player. Using this idea, SHAP breaks down the prediction for a specific patient u represented as $f\left(y^{(u)}\right)$ into a sum of individual contributions from each feature (j), written as $\phi_j\left(y_j^{(u)}\right)$. This helps clearly understand how each input, such as clinical and image patterns, affects diagnosis.

$$\phi_0 = \frac{1}{V}\sum_{u=1}^{V} f\left(y^{(u)}\right) \quad (23)$$

$$\phi_j\left(y_j^{(u)}\right) = \Phi\left(y_j^{(u)}\right) - \frac{1}{V}\sum_{R=1}^{V}\Phi\left(y_j^{(R)}\right) \quad (26)$$

$$f\left(y^{(u)}\right) = \phi_0 + \sum_{j=1}^{R}\phi\left(y_j^{(u)}\right) \quad (27)$$

where, V represents the total amount of patients in the dataset. From equation 24, it is shown that for every feature j, the average SHAP value across all diseases is zero. This means that SHAP values are balanced across the dataset.

3.5 Secured dual stage Encryption System Technique Using Elgamal ECC

The security technique used in this system relies on the mathematical difficulty of solving discrete logarithm problems involving very large prime numbers, making it highly secure against unauthorized access. An important feature of this method is that even if the same patient information (plaintext) is encrypted multiple times, the resulting encrypted outputs (Ciphertexts) will be different each time, adding an extra layer of protection.

The ElGamal encryption process used to secure classified patient data involves three steps:

- **Key Generation:** Creating public and private keys based on large prime values
- **Encryption:** Converting sensitive patient information into a secure, unreadable form using the public key.
- **Decryption:** Recovering the original information using the corresponding private key.

3.5.1 Key Generation

- First, choose a large random prime number q along with two other random values y, h ensuring both y and h are smaller than q.
- Then compute z using the equation:

  $z = h^y \mod q$ (28)

  This means raising h to the power of y and taking the remainder after dividing by q.
- The combination (q, h, z) forms the public key, which can be shared openly, i.e., secured cloud based hospital systems.
- The value y, is kept private a remains known only to the authorized system. It serves as the secret key for decrypting sensitive patient results, such as cancer classification outcomes.

3.5.2 Encryption / Decryption process

To securely encrypt a patient's classified result (message n), the following steps are performed:

1. A random number L is selected such that it shares no common factors with $(q-1)$, ensuring it's mathematically compatible for encryption.
2. Next, the encrypted output is created as a pair of values $(D1, D2)$ using these formulas:

$$D1 = hL \bmod q \quad (29)$$

$$D2 = (zL \times n) \quad (30)$$

3. This cipher text pair $(D1, D2)$ is what gets transmitted or stored, i.e., when saving diagnostic results to the cloud.

To decrypt and retrieve the original patient data, the private key y is used with the equation:

$$n = \frac{D2}{(D1\,y) \bmod q} \quad (31)$$

This process securely recovers the original message n (lung cancer result) without exposing it during transmission or storage.

Algorithm 1

Encryption stage:

$ELGamalEncry(f1, f2, q, Q)$ // Q is the plain text

{

Select a random integer s in the group $H =< A_q *, y >$

$D1 \leftarrow f_1^s \bmod q$

$D2 \leftarrow (Q \times f_2^s) \bmod q$

$return\ D1\ and\ D2$

} // $D1$ and $D2$ are the cipher texts

Algorithm 2

Decryption stage:

$ElGamalDecypt(e, q, D1, D2)$ // $D1$ and $D2$ are the cipher texts

{

$q \leftarrow \left[D2(D_1^e)^{-1}\right] \bmod q$ // Q is the plain text

$return\ Q$

Algorithm 3

$ElGamal\_keyGener$

{

Select a large prime number q

Select e to be a member of the group $H =< A_q *, y >$ such that $1 \le e \le q-2$

Select $f1$ to be a primitive root in the group $H =< A_q *, y >$

$f2 \leftarrow f_1^e \bmod q$

$pubKey \leftarrow (f1, f2, q)$ // To be announced publicly

$priKey \leftarrow e$ // To be kept secret

Return $PubKey \ \ and \ \ \Pr iKey$

}

4. Result and Discussion

This section presents the outcomes and evaluation of the suggested multimodal lung cancer classification framework. It provides an exploration setup, details about the medical imaging and genomic datasets used for testing, and the performance metrics applied to evaluate the accuracy and efficacy of the classification model [33]. This deep learning model effectively secured the data through SHAP using Elgamal ECC to secure the patients data is assessed and discussed. Table 3 summarizes the hardware and software environment used to execute and test the proposed model.

Table 3: System Configuration

Components	Details
Processor	Intel® Core i5-6500 CPU @ 3.20GHz 3.19 GHz
RAM	16.0 GB (15.9 GB usable)
System Type	64-bit operating system, x64-based processor

4.1 Dataset Description

This proposed model utilized Clinical data from the TCIA repository [31], which contains computed Tomography images (CT) of the mediastinum and abdomen in which radiologists mark lymph node locations. Radiologists labeled a total of 388 mediastinal lymph nodes in CT images of 90 patients and a total of 595 abdominal lymph nodes in 86 patients. Genomic data is gathered from the TCGA repository [32] contains diseases of Acinar cell Neoplasms, Adenomas and Adenocarcinomas, Cystic, Mucinous and serous Neoplasms, Ductal and Lobular Neoplasms. In this study 80% of the data was utilized for training and 20% for assessing the dataset.

4.2 Performance Metrics

The performance of the proposed classification model was assessed employing multiple quantitative metrics, including accuracy, precision, recall, F1-score, and so on. Performance metrics descriptions are described below:

$$Accuracy = \frac{(PT + NT)}{(PT + NT + PF + FN)} \quad (32)$$

$$\Pr ecision = \frac{PT}{PT + PF} \quad (33)$$

$$\mathrm{Re}\, call = \frac{PT}{PT + NF} \quad (34)$$

$$F - score = \frac{2 \times (\Pr ecision \times \mathrm{Re}\, call)}{(\Pr ecision + \mathrm{Re}\, call)} \quad (35)$$

where, PT, NT, PF, and NF are True positives, True Negatives, False Positives, and False Negatives, correspondingly.

4.3 Performance Evaluation

To evaluate the performance of the proposed approach, it was tested on a clinical and genomic dataset. The resulting performance was benchmarked against existing models, ViT [27], CNN-ViT [28], Trans-MSDL [29], and FocalNext [30]. Figure 6illustrates the accuracy of both datasets with existing models.

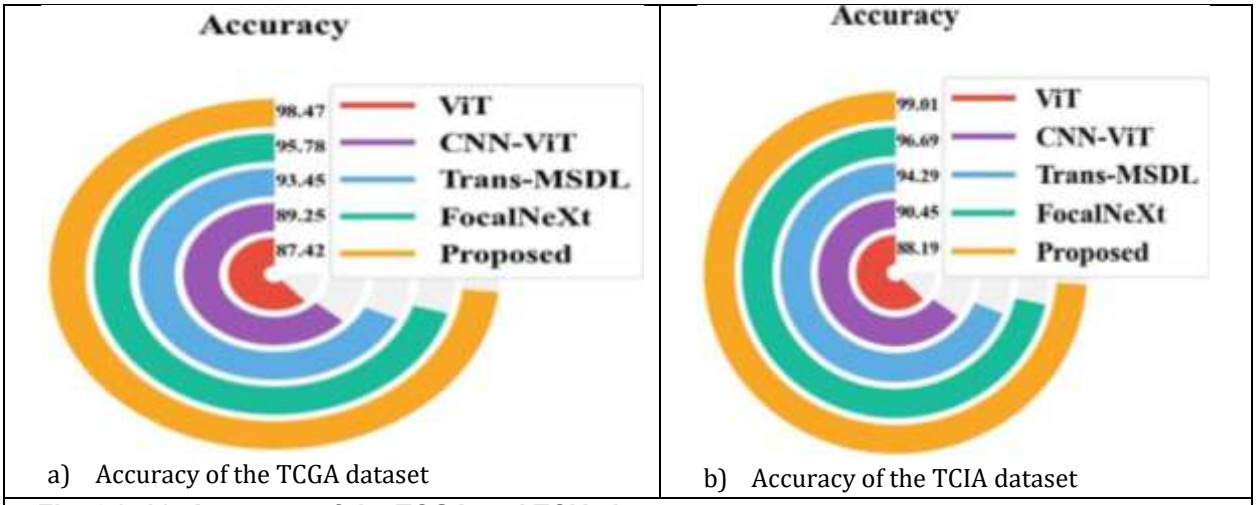

a) Accuracy of the TCGA dataset

b) Accuracy of the TCIA dataset

Fig. 6 (a-b): Accuracy of the TCGA and TCIA datasets

This graph compares the classification accuracy of four different models with the proposed model on two datasets. The TCGA dataset attained an accuracy of 98.47% and the TCIA dataset attained the highest accuracy of 99.01%, outperforming ViT, CNN-ViT, Trans-MSDL, and FocalNeXt. Among the existing models, CNN-ViT comes next with 95.78% and 96.69% accuracy. The graph clearly shows the efficacy of the suggested method in providing superior predictive performance. Figure 7 compares the precision of the suggested and the present system for both datasets.

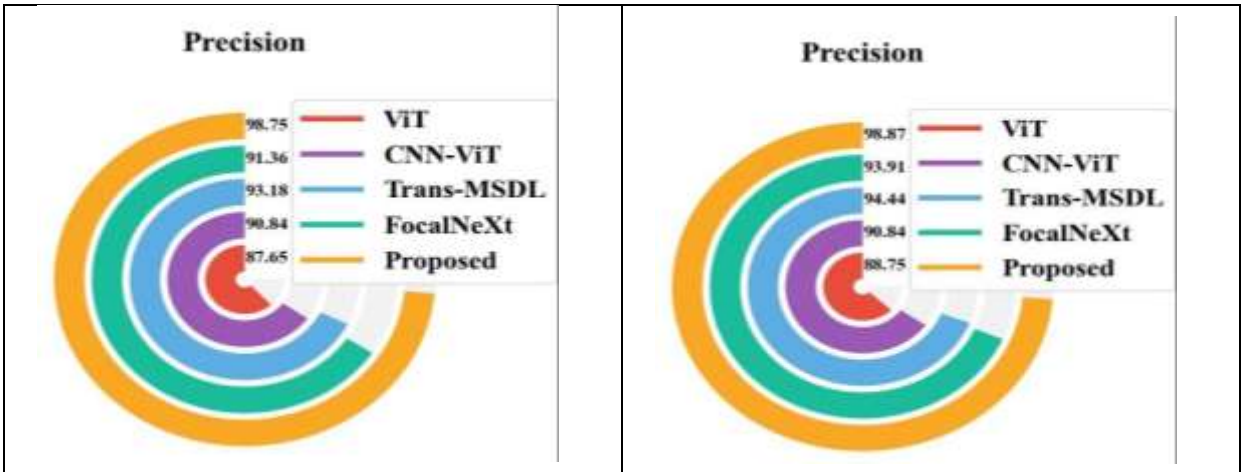

a) Precision of the TCGA dataset

b) Precision of the TCIA dataset

Fig. 7 (a-b): Precision of the TCGA and TCIA datasets

The graph compares the precision of four current models to the suggested model. The suggested model has the highest precision (98.75% and 98.87%), greatly surpassing the others. Among the rest, the precision of Trans-MSDL among both datasets is 93.18% and 94.44%. Further, the precision of CNN-ViT is 91.36% and 93.91%. This demonstrates the proposed model's superior ability to correctly recognize true positives. Figure8illustrates the Recall and F1-score of the proposed system with the existing system for both datasets.

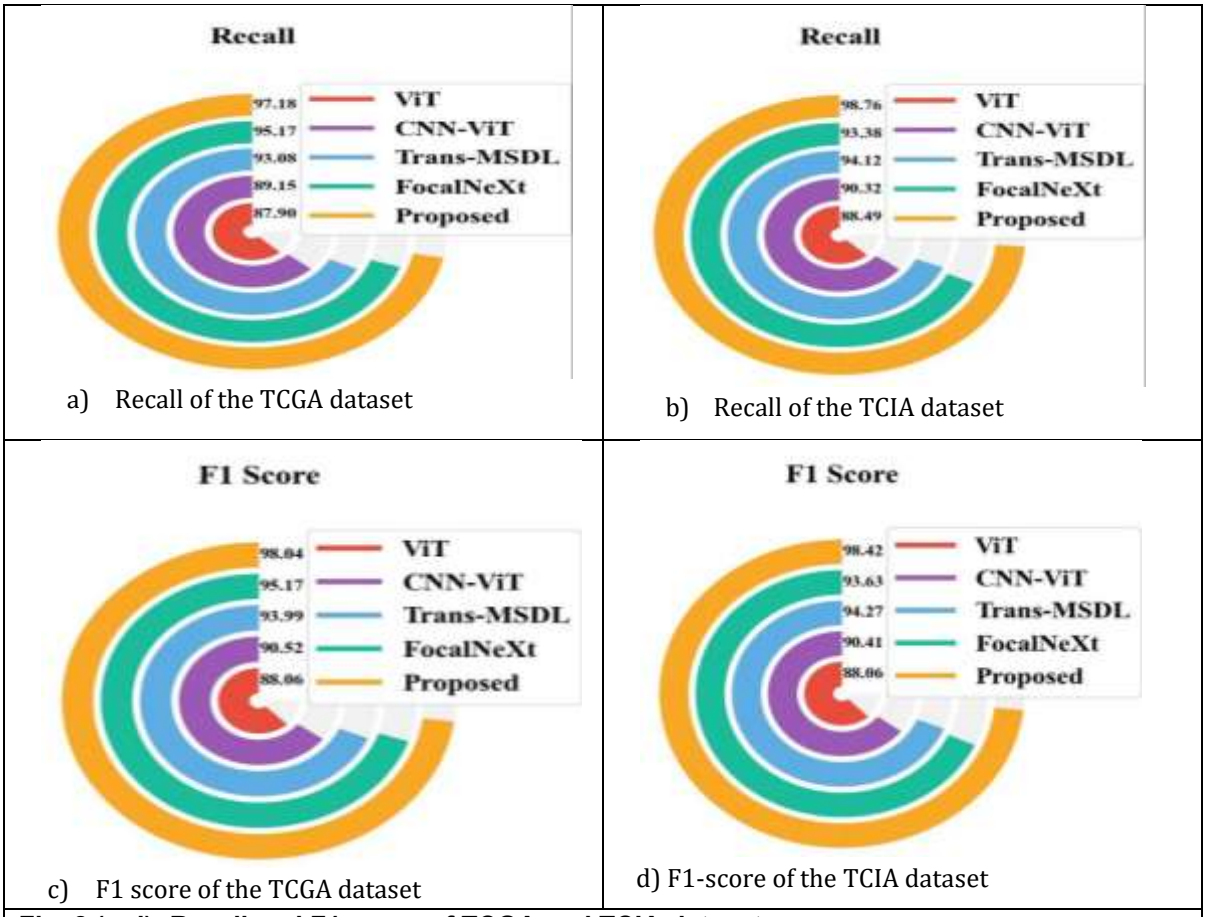

a) Recall of the TCGA dataset

b) Recall of the TCIA dataset

c) F1 score of the TCGA dataset

d) F1-score of the TCIA dataset

Fig. 8 (a-d): Recall and F1-score of TCGA and TCIA datasets

This graph shows the recall and F1-score with the comparison of the existing model with the suggested model. This model achieves a highest recall of 97.18% and 98.76%, indicating its strong ability to detect true positive cases. It surpasses CNN-ViT and Trans-MSDL. This highlights the model's effectiveness in capturing all relevant cases of the condition. In the F1-score comparison, the proposed model again leads with 98.04% and 98.42%, reflecting a balanced performance between recall and F1-score. F1-score of CNN-ViT and Trans-MSDL among the TCGA dataset is 95.17% and 93.99% respectively. Further, F1-score on the TCIA dataset of CNN-ViT and Trans-MSDL models is 93.63% and 94.27% correspondingly. These outcomes confirm that the suggested approach delivers consistent and reliable classification. Figure 9illustrates the execution time of the suggested model with the current model.

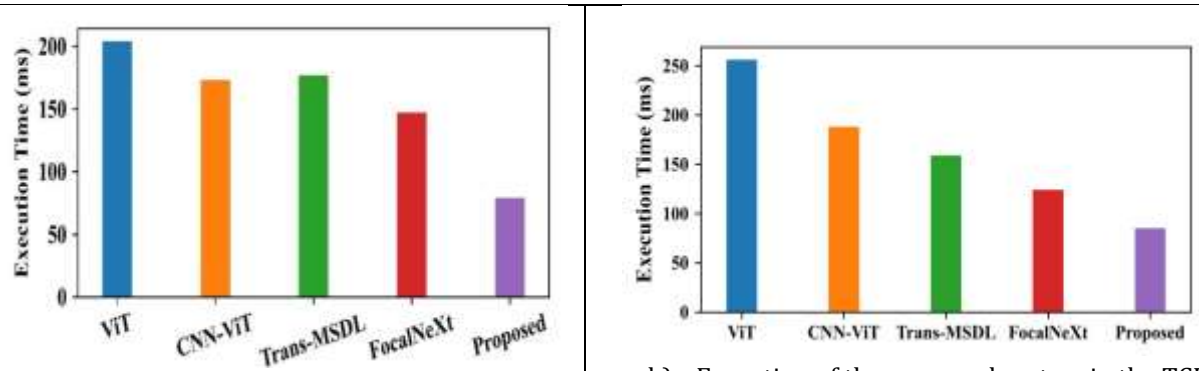

a) Execution of the proposed system in the TCGA dataset

b) Execution of the proposed system in the TCIA dataset

Fig. 9 (a-b): Execution time of the proposed system with two datasets

This bar graph compares the execution time of four current models with the suggested model for both datasets. The proposed model has the lowest execution time, making it the most efficient in terms of speed. In contrast, ViT takes the longest time, exceeding 200ms. The result shows the proposed method is both fast and resource efficient for real-time deployment. Figure 10 illustrates the training accuracy of both datasets proposed with existing models.

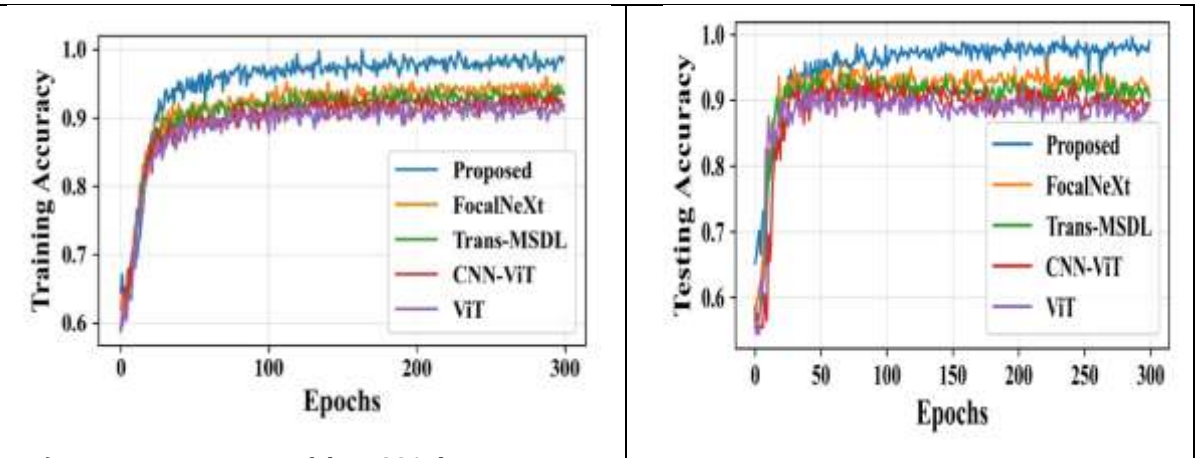

a) Training accuracy of the TCGA dataset

b) Training accuracy of the TCIA dataset

Fig. 10 (a-b): Training accuracy of the TCGA and TCIA datasets

The line graph shows the training accuracy over 300 epochs for four existing models and with proposed model. The proposed model consistently outperforms others, reaching the highest accuracy. Other models like Focal NeXT, Trans-MSDL, and CNN-ViT stabilize at lower accuracy levels. The result highlights the superior learning capability of the proposed framework. Figure 11illustrates the testing accuracy of both datasets.

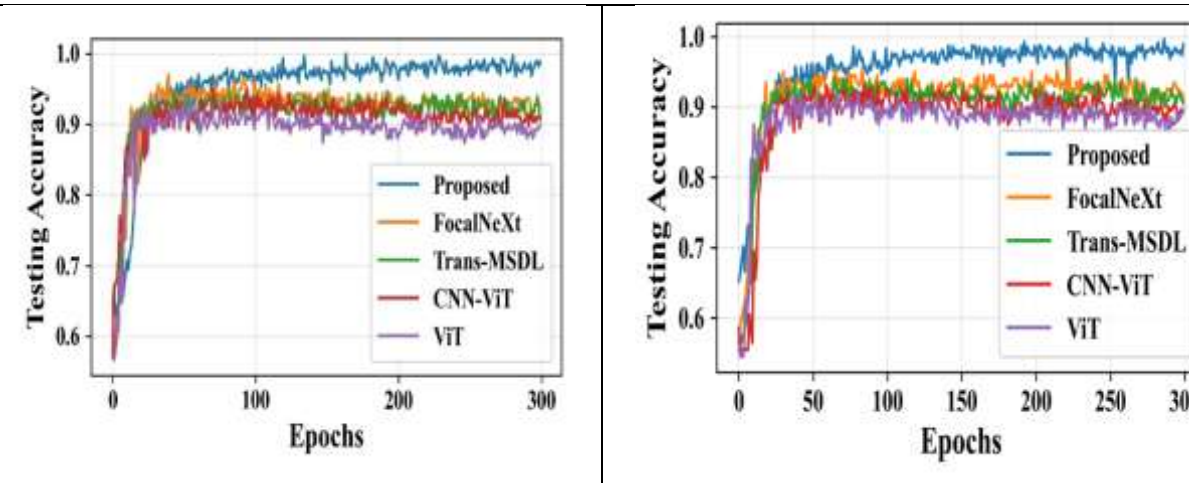

a) Testing the accuracy of the TCGA dataset

b) Testing the accuracy of the TCIA dataset

Fig. 11 (a-b): Testing accuracy of the TCGA and TCIA datasets

The graph shows the testing accuracy of both datasets. The proposed model outperforms the existing four models. Existing models like FocalNeXt, Trans-MSDL, CNN-ViT, and ViT have lower testing accuracy. The suggested model has the highest testing accuracy. Figure 12shows the comparison of training loss and testing loss of the proposed model with existing models.

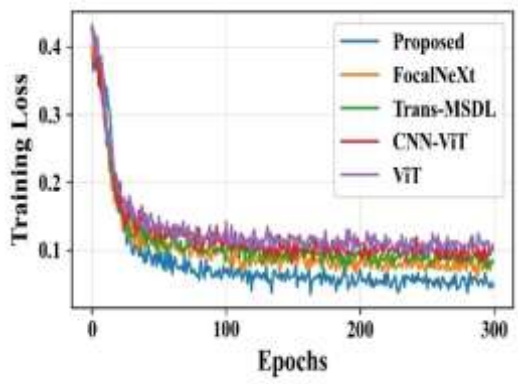

a) Training loss of TCGA

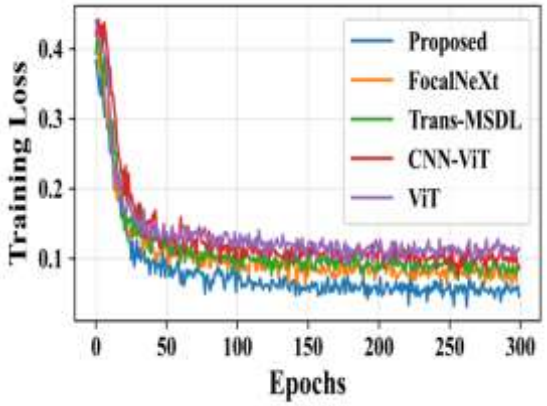

b) Training loss of TCIA

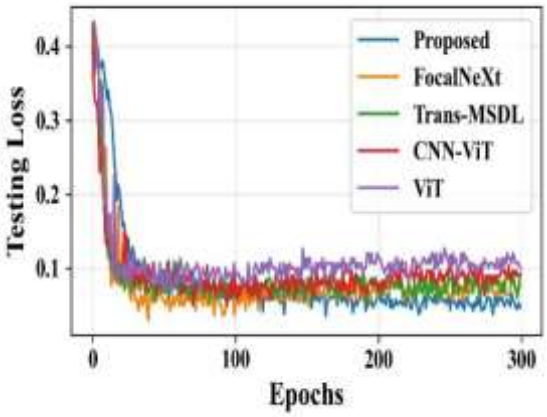

c) Testing loss of TCGA

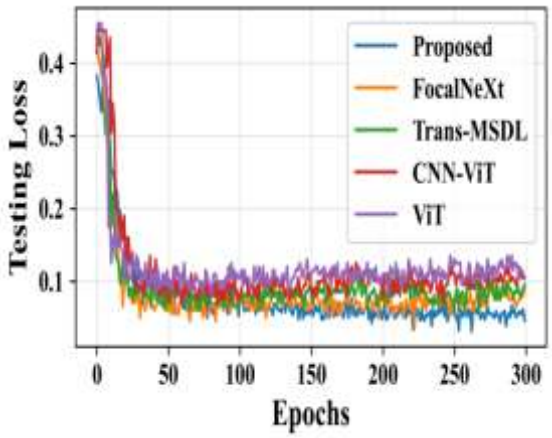

d) Training loss of TCIA

Fig. 12 (a-d): Training and testing loss of the TCGA and TCIA datasets

The above line graphs explore the Training and Testing loss of the TCGA and TCIA datasets. The proposed model achieves the lowest and stable loss, indicating better convergence and learning. Other models show relatively higher and more fluctuating loss values. This demonstrates the proposed model's superior optimization and training efficiency. Figure 13 illustrates the ROC curve of both datasets with the proposed and existing models.

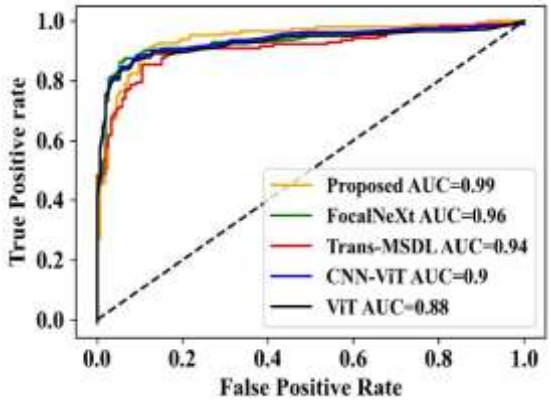

a) ROC of the TCGA dataset

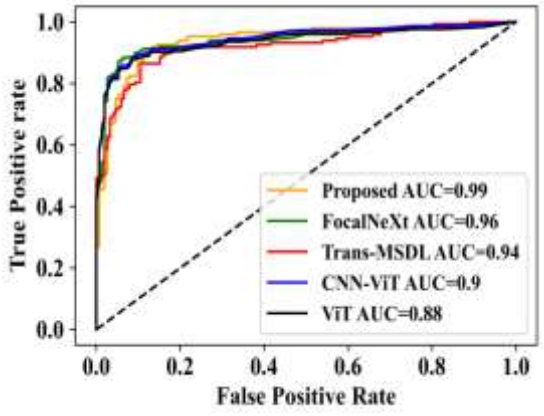

b) ROC of the TCIA dataset

Fig. 13 (a-b): ROC of the TCGA and TCIA datasets

This ROC curve compares the AUC (Area under Curve) scores of five models for classification performance. The proposed model achieves the highest AUC of 0.99, indicating excellent sensitivity and specificity. Other models, like FocalNeXt (0.96) and Trans-MSDL (0.94), perform slightly slower. This confirms the proposed method's strong capability in distinguishing between classes. Figure 14 illustrates the Encryption time of the data to transfer into the cloud.

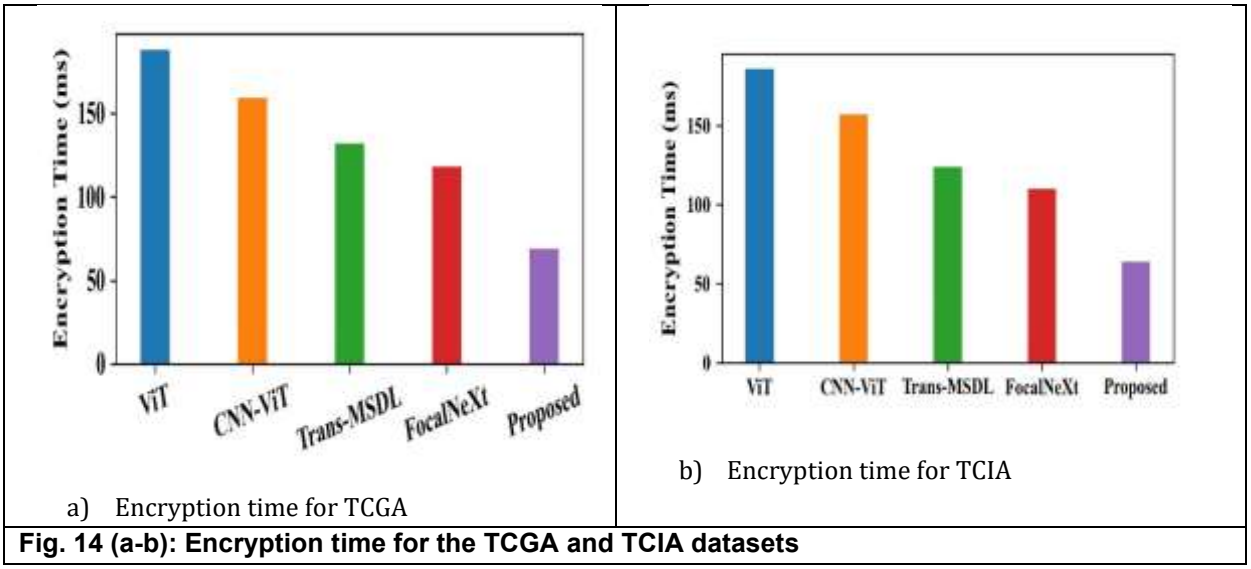

a) Encryption time for TCGA

b) Encryption time for TCIA

Fig. 14 (a-b): Encryption time for the TCGA and TCIA datasets

The bar graph compares the encryption time of four existing models with the proposed model. The proposed method shows faster encryption in both datasets, while ViT has the slowest performance. Other models like CNN-ViT and Trans-MSDL fall in between. This demonstrates the proposed system's efficiency in securing data quickly for cloud –based storage transmission. Table 4 demonstrates the performance evaluation of the suggested system with the current system.

Table 4: Comparison of the proposed system with existing systems

Models	Accuracy %	Precision %	F1-score%	Recall %	Encryption time (ms)	Execution time (ms)
ViT	87.42	87.65	88.06	87.9	188	204
CNN-ViT	89.25	90.84	93.99	93.08	159	173
Trans-MSDL	93.45	93.18	93.99	93.08	132	177
FocalNeXt	95.78	91.36	95.17	95.17	118	147
Proposed model	**98.47**	**98.75**	**98.04**	**97.18**	**69**	**79**

Table 4 compares the performance evaluation of the suggested system with the current system. The accuracy of the suggested system is 98.47, precision is 98.75, F1-score is 98.04, recall is 97.18, Encryption time is 69 ms, and it takes an execution time of 79 ms, which demonstrates the high performance compared to the existing models.

Table 5: Performance evaluation of the proposed system with existing systems

Models	Accuracy %	Precision %	F1-score%	Recall %	Encryption time (ms)	Execution time (ms)
ViT	88.19	88.75	88.06	88.49	186	256
CNN-ViT	90.45	90.84	90.41	90.32	157	188
Trans-MSDL	94.29	94.44	94.27	94.12	124	159
FocalNeXt	96.69	93.91	93.63	93.38	110	124
Proposed model	**99.01**	**98.87**	**98.42**	**98.76**	**64**	**85**

Table 5 demonstrates the performance evaluation of various methods. The accuracy of the suggested system is 99.01%, precision is 98.87%, F1-score is 98.42%, recall is 98.76%, Encryption time is 64 ms, and it takes an execution time of 85 ms, which shows the high performance compared to the existing models.

4.4 Discussion

In this research, a novel framework for early lung cancer detection employing multimodal medical data and efficient deep learning feature extractors is developed. By leveraging recent progress in medical image analysis and efficient storage of data, the proposed method successfully overcomes the challenges and limitations observed in earlier diagnostic models. Further, [18] developed a deep learning model, but there is no efficient classification model used; this system utilized an efficient model of CDF-NPT. A machine learning model was developed by [19]. This system is computationally very high, while this proposed model is computationally low. The RCNN model was suggested by [20], where this model was trained using a small dataset, while the suggested model was trained employing two datasets. The CNN model was suggested by [21], but it needs to train the model using advanced methods, whereas this proposed system utilized advanced deep models to overcome the limitations. A machine learning model was developed by [22], where this system needs to enhance the dataset and accuracy, while the proposed system utilized a large dataset and attained high accuracy. Similarly, [23] consumes more processing time, but this proposed system utilizes the CDF-NPT pruning method to reduce the processing time. An Artificial Intelligence model was suggested by [24], where this model has low accuracy, but this proposed system utilized an effective pruning method to improve the accuracy. Likewise, [25] developed a deep learning model of MobileNetV2; however, this model needs to enhance its application. This proposed model enhanced the application by enabling accurate and secure early lung cancer detection through a multimodal dataset. Similarly, [26] developed a machine learning model, but the processing time is high; his proposed system takes a low processing time of 79 ms. Table 6 illustrates the comparison of various methods.

Table 6: Comparison of the proposed system with the existing system

Author Name	Accuracy
Wankhade et al. [18]	95%
Bhuiyan et al. [19]	92%
Srivastava et al. [20]	97%
Mamun et al. [21]	92%
Naseer et al. [22]	97.64%
Noaman et al. [23]	97.683%
Verma et al. [24]	95%
Ochoa-Ornelas et al. [25]	98.11%
Al-Jamimi et al. [26]	98%
Proposed model	98.47%
	99.01%

5. Conclusions

The proposed system demonstrates high accuracy in correctly identifying several kinds of lung cancer in patients. Previously, studies have aimed to increase the precision and reliability of cancer diagnosis. Building on these efforts, this approach introduces a deep learning based-model that utilizes multimodal medical data to detect early signs of abnormalities in lung tissues, improving early-stage diagnosis. Initially, the images are pre-processed, and in the raw image, the missing values are imputed using the Mean imputation method. Features are extracted utilizing PyRadiomics, Principal Component Analysis, and t-Distributed Stochastic Neighbor embedding, and deep features are extracted using Residual AlexNet; clinical data is encoded using one-hot encoding. The extracted features are classified using the CDF-NPT framework, and for the feature attribution framework, the SHAP framework was used. Finally, the data was encrypted to securely store the patient data in the cloud. In the performance evaluation, the proposed system attained an accuracy of 98.47% and 99.01%, precision of 98.75%, 98.87% and Encryption time of 69 ms, 64 ms, respectively. Future scope is to enhance this model by storing the patient's data in blockchain technology for more security.

References

1. Nivashini, A., and M. Krishnamurthy. "Revolutionizing lung cancer classification through Artificial Intelligence: A Concise review." *Expert Systems with Applications* (2025): 128508.
2. Ren, Zeyu, Yudong Zhang, and Shuihua Wang. "A hybrid framework for lung cancer classification." *Electronics* 11, no. 10 (2022): 1614.
3. Nanglia, Pankaj, Sumit Kumar, Aparna N. Mahajan, Paramjit Singh, and Davinder Rathee. "A hybrid algorithm for lung cancer classification using SVM and Neural Networks." *ICT Express* 7, no. 3 (2021): 335-341.
4. Pandit, Bhoj Raj, Abeer Alsadoon, P. W. C. Prasad, Sarmad Al Aloussi, Tarik A. Rashid, Omar Hisham Alsadoon, and Oday D. Jerew. "Deep learning neural network for lung cancer classification: enhanced optimization function." *Multimedia Tools and Applications* 82, no. 5 (2023): 6605-6624.
5. Katar, Oguzhan, Ozal Yildirim, Ru-San Tan, and U. Rajendra Acharya. "A Novel Hybrid Model for Automatic Non-Small Cell Lung Cancer Classification Using Histopathological Images." *Diagnostics* 14, no. 22 (2024): 2497.
6. Kwon, Hyuk-Jung, Ui-Hyun Park, Chul Jun Goh, Dabin Park, Yu Gyeong Lim, Isaac Kise Lee, Woo-Jung Do et al. "Enhancing lung cancer classification through integration of liquid biopsy multi-omics data with machine learning techniques." *Cancers* 15, no. 18 (2023): 4556.
7. Naseer, Iftikhar, Sheeraz Akram, Tehreem Masood, Muhammad Rashid, and Arfan Jaffar. "Lung cancer classification using modified u-net based lobe segmentation and nodule detection." *IEEE Access* 11 (2023): 60279-60291.
8. Chen, Ying, Yerong Wang, Fei Hu, Longfeng Feng, Taohui Zhou, and Cheng Zheng. "LDNNET: towards robust classification of lung nodule and cancer using lung dense neural network." *IEEE Access* 9 (2021): 50301-50320.
9. Mohamed, Tehnan IA, and Absalom El-Shamir Ezugwu. "Enhancing lung cancer classification and prediction with deep learning and multi-omics data." *IEEE Access* 12 (2024): 59880-59892.
10. Li, Min, Xiaojian Ma, Chen Chen, Yushuai Yuan, Shuailei Zhang, Ziwei Yan, Cheng Chen et al. "Research on the auxiliary classification and diagnosis of lung cancer subtypes based on histopathological images." *Ieee Access* 9 (2021): 53687-53707.
11. Sangeetha, S. K. B., Sandeep Kumar Mathivanan, P. Karthikeyan, Hariharan Rajadurai, Basu Dev Shivahare, Saurav Mallik, and Hong Qin. "An enhanced multimodal fusion deep learning neural network for lung cancer classification." *Systems and Soft Computing* 6 (2024): 200068.
12. Wang, Lulu. "Deep learning techniques to diagnose lung cancer." *Cancers* 14, no. 22 (2022): 5569.
13. Mahum, Rabbia, and Abdulmalik S. Al-Salman. "Lung-RetinaNet: Lung cancer detection using a RetinaNet with multi-scale feature fusion and context module." *IEEE Access* 11 (2023): 53850-53861.
14. Obayya, Marwa, Munya A. Arasi, Nuha Alruwais, Raed Alsini, Abdullah Mohamed, and Ishfaq Yaseen. "Biomedical image analysis for colon and lung cancer detection using tuna swarm algorithm with deep learning model." *IEEE Access* 11 (2023): 94705-94712.
15. Sreeprada, V., and K. Vedavathi. "Lung Cancer Detection from X-Ray Images using Hybrid Deep Learning Technique." *Procedia Computer Science* 230 (2023): 467-474.
16. Navaneethakrishnan, M., M. Vijay Anand, G. Vasavi, and V. Vasudha Rani. "Deep Fuzzy SegNet-based lung nodule segmentation and optimized deep learning for lung cancer detection." *Pattern Analysis and Applications* 26, no. 3 (2023): 1143-1159.
17. Prasad, Umesh, Soumitro Chakravarty, and Gyaneshwar Mahto. "Lung cancer detection and classification using deep neural network based on hybrid metaheuristic algorithm." *Soft Computing* 28, no. 15 (2024): 8579-8602.
18. Wankhade, Shalini, and S. Vigneshwari. "A novel hybrid deep learning method for early detection of lung cancer using neural networks." *Healthcare Analytics* 3 (2023): 100195.
19. Bhuiyan, Mohammad Shafiquzzaman, Imranul Kabir Chowdhury, Mahfuz Haider, Afjal Hossain Jisan, Rasel Mahmud Jewel, Rumana Shahid, Mst Zannatun Ferdus, and Cynthia Ummay Siddiqua. "Advancements in early detection of lung cancer in public health: a comprehensive study utilizing machine learning algorithms and predictive models." *Journal of Computer Science and Technology Studies* 6, no. 1 (2024): 113-121.
20. Srivastava, Durgesh, Santosh Kumar Srivastava, Surbhi Bhatia Khan, Hare Ram Singh, Sunil K. Maakar, Ambuj Kumar Agarwal, Areej A. Malibari, and Eid Albalawi. "Early Detection of Lung Nodules Using a Revolutionized Deep Learning Model." *Diagnostics* 13, no. 22 (2023): 3485.
21. Mamun, Muntasir, Md Ishtyaq Mahmud, Mahabuba Meherin, and Ahmed Abdelgawad. "Lcdctcnn: Lung cancer diagnosis of ct scan images using cnn based model." In *2023 10th International Conference on Signal Processing and Integrated Networks (SPIN)*, pp. 205-212. IEEE, 2023.

22. Naseer, Iftikhar, Tehreem Masood, Sheeraz Akram, Arfan Jaffar, Muhammad Rashid, and Muhammad Amjad Iqbal. "Lung Cancer Detection Using Modified AlexNet Architecture and Support Vector Machine." *Computers, Materials & Continua* 74, no. 1 (2023).
23. Noaman, Naglaa F., Bassam M. Kanber, Ahmad AL Smadi, Licheng Jiao, and Mutasem K. Alsmadi. "Advancing oncology diagnostics: AI-enabled early detection of lung cancer through hybrid histological image analysis." *IEEE Access* (2024).
24. Verma, Saher, Leander Maerkisch, Alberto Paderno, Leonard Gilberg, Bianca Teodorescu, and Mathias Meyer. "One Scan, Multiple Insights: A Review of AI-Driven Biomarker Imaging and Composite Measure Detection in Lung Cancer Screening." *Meta-Radiology* (2025): 100124.
25. Ochoa-Ornelas, Raquel, Alberto Gudiño-Ochoa, Julio Alberto García-Rodríguez, and Sofia Uribe-Toscano. "Enhancing early lung cancer detection with MobileNet: A comprehensive transfer learning approach." *Franklin Open* (2025): 100222.
26. Al-Jamimi, Hamdi A., Sarah Ayad, and Ammar El Kheir. "Integrating Advanced Techniques: RFE-SVM Feature Engineering and Nelder-Mead Optimized XGBoost for Accurate Lung Cancer Prediction." *IEEE Access* (2025).
27. Imran, Muhammad, Bushra Haq, Ersin Elbasi, Ahmet E. Topcu, and Wei Shao. "Transformer Based Hierarchical Model for Non-Small Cell Lung Cancer Detection and Classification." *IEEE Access* (2024).
28. Qiu, Jianwei, Jhimli Mitra, Soumya Ghose, Camille Dumas, Jun Yang, Brion Sarachan, and Marc A. Judson. "A multichannel CT and radiomics-guided CNN-ViT (RadCT-CNNViT) ensemble network for diagnosis of pulmonary sarcoidosis." *Diagnostics* 14, no. 10 (2024): 1049.
29. Zhu, PengFei, TingMin Wang, Fan Yang, Meng Wang, and YunJie Zhang. "A Transformer-Based Multi-Scale Deep Learning Model for Lung Cancer Surgery Optimization." *IEEE Access* (2025).
30. Gulsoy, Tolgahan, and Elif Baykal Kablan. "FocalNeXt: A ConvNeXt augmented FocalNet architecture for lung cancer classification from CT-scan images." *Expert Systems with Applications* 261 (2025): 125553.
31. https://doi.org/10.7937/K9/TCIA.2015.AQIIDCNM
32. https://portal.gdc.cancer.gov/projects/TCGA-LUAD
33. Thamilarasi V., Roselin. R., Automatic Classification and Accuracy by Deep Learning Using CNN Methods in Lung Chest X-Ray Image, IOP Conf. Ser.: Mater. Sci. Eng. 1055 012099.(2020).